Struct Multidisc Optim (2012) 46:285–301
DOI 10.1007/s00158-011-0756-2

RESEARCH PAPER

Inverse and direct magnetic shaping problems

Jaemin Shin · John P. Spicer · Jeffrey A. Abell

Received: 27 June 2011 / Revised: 26 November 2011 / Accepted: 20 December 2011 / Published online: 26 January 2012

Abstract In this work, we study the direct and inverse problems arising from electromagnetic shaping in applications such as continuous casting processes. The magnetic field produces a surface pressure which forces a molten metal to change its shape until it reaches an equilibrium state between the magnetic pressure and the surface tension. The arising direct problem is a free boundary problem which is to determine the shape of molten metals for a given magnetic field. On the other hand, the inverse problem is to seek a configuration of electromagnetic field generators (i.e. inductors) in order that molten metals have prescribed shapes. A level set method will be presented to determine an equilibrium shape formed by a given configuration of magnetic fields. Also a computational method as well as uniqueness results for the inverse problem will be introduced and illustrated with examples.

Keywords Inverse shaping problem · Electromagnetic casting · Inverse source problem · Free boundary problem · Level set method

J. Shin (✉)
Department of Mathematics, Wayne State University, Detroit, MI 48202, USA
e-mail: jaemin.shin@wayne.edu

J. P. Spicer · J. A. Abell
General Motors Global Research and Development, 30500 Mound Road, Warren, MI 48090, USA

J. P. Spicer
e-mail: patrick.spicer@gm.com

J. A. Abell
e-mail: jeffrey.abell@gm.com

1 Introduction

Traditional manufacturing processes require custom-built tooling, such as dies or molds, to form materials into specific shapes. By contrast, electromagnetic shaping in applications such as continuous casting processes offers the potential to manufacture parts without using hard tooling. The benefits of eliminating hard tooling include enhanced operational flexibility and tooling cost reduction. In this work, we analyze the mathematical model and give numerical simulation results for electromagnetic shaping of homogeneous materials (e.g. molten metals) in 2-dimensional space.

Suppose that there is an infinitely long vertical cylinder that contains a layer of molten metal surrounded by a set of inductors under vacuum. Then the surface of the molten metal is shaped by the electromagnetic force from the inductors. We assume that the frequency of the current in the inductors is very high so that the magnetic field does not penetrate into the metal. If we ignore the perturbation of the cylinder which occurs under gravity, the problem can be treated as a 2-dimensional problem by considering a cross section of the cylinder (Shercliff 1981). Some results for a 3-dimensional problem including gravity can be found in literature (e.g. Pierre and Roche 1993; Pierre and Rouy 1996).

It is known (see e.g. Shercliff 1981; Pierre and Roche 1991) that the following system of equations on a cross section of the cylinder represents the equilibrium state between the Laplace force and the magnetic pressure at the boundary of the domain, which is the interface of the molten metal and the vacuum (see Fig. 1a).

$$\nabla \times \mathbf{B} = \mu_0 \mathbf{j} \quad \text{in } \Omega \tag{1.1a}$$

$$\nabla \cdot \mathbf{B} = 0 \quad \text{in } \Omega \tag{1.1b}$$

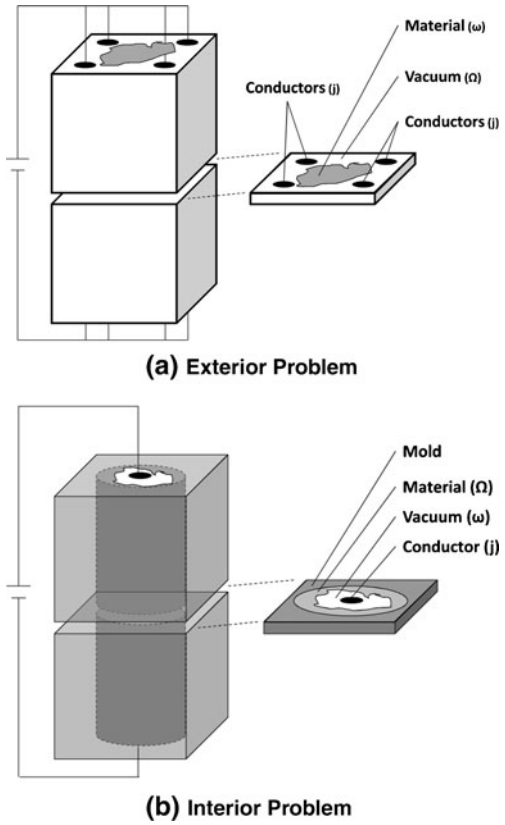

Fig. 1 Example magnetic shaping apparatuses showing two different types of shaping problems: **a** The exterior problem where shaping conductors are outside of the material. **b** The interior problem where shaping conductors are inside of the material

$$\mathbf{B} \cdot \nu = 0 \quad \text{on } \Gamma \tag{1.1c}$$

$$|\mathbf{B}| = O\left(\frac{1}{|x|^2}\right) \quad \text{as } |x| \to \infty \tag{1.1d}$$

$$\frac{1}{2\mu_0}|\mathbf{B}|^2 + \sigma\kappa = P_0 \quad \text{on } \Gamma \tag{1.1e}$$

Here $\mathbf{B} = (B_{x^{(1)}}, B_{x^{(2)}}, 0)$ is the magnetic field, $\mathbf{j} = (0, 0, j)$ the density of the current vector such that

$$\int_\Omega j dx = 0, \tag{1.2}$$

ν the unit normal vector from the bounded domain $\omega := \overline{\Omega}^c$ to Ω at the boundary $\Gamma := \partial\omega$, μ_0 the magnetic permeability, σ the surface tension of the molten metal, κ the curvature of Γ, and P_0 a constant which represents the difference between the interior and exterior pressures. We assume further that j is compactly supported in Ω. Then there exists a potential function u such that

$$\mathbf{B} = \left(\frac{\partial u}{\partial x^{(2)}}, -\frac{\partial u}{\partial x^{(1)}}, 0\right)$$

and solves

$$-\Delta u = \mu_0 j \quad \text{in } \Omega \tag{1.3a}$$

$$u = 0 \quad \text{on } \Gamma \tag{1.3b}$$

$$\left|\frac{\partial u}{\partial r}\right| = O\left(\frac{1}{|x|^2}\right) \quad \text{as } |x| \to \infty \tag{1.3c}$$

$$\frac{1}{2\mu_0}|\nabla u|^2 + \sigma\kappa = P_0 \quad \text{on } \Gamma \tag{1.3d}$$

where $r = |x|$. If it is assumed that the molten metal is incompressible, the area of the cross section should be fixed. Thus we have the following additional condition for a given S_0.

$$\int_\omega dx = S_0. \tag{1.4}$$

Another well-known mathematical model for the electromagnetic casting of molten metals is an interior problem, which reads

$$-\Delta u^i = \mu_0 j \quad \text{in } \omega \tag{1.5a}$$

$$u^i = 0 \quad \text{on } \Gamma \tag{1.5b}$$

$$\frac{1}{2\mu_0}|\nabla u^i|^2 - \sigma\kappa = P_0 \quad \text{on } \Gamma \tag{1.5c}$$

$$\int_\omega dx = S_0 \tag{1.5d}$$

Here we assume that the simply connected domain ω is surrounded by materials and the set of inductors is located in ω (see Fig. 1b).

It is a free boundary problem to determine Γ for a given current density j from (1.3) or (1.5). This free boundary problem or problems with similar boundary condition to (1.3d) and (1.5c) have been studied analytically as well as numerically. Especially, Henrot and Pierre found necessary and sufficient condition for the existence for the exterior problem (1.1) under certain restrictions on j and P_0 using the technique of complex potentials in Henrot and Pierre (1989) (see also Canelas et al. 2009b). A variational formulation for (1.3) and (1.5) was introduced in Pierre and Roche (1991) (see also Crouzeix 1991), which is one of the key ingredients in the literature. Define a functional

$$E^o(\omega) = -\frac{1}{2\mu_0}\int_\Omega |\nabla u|^2 dx + \sigma\int_\Gamma dS \tag{1.6}$$

where u solves (1.3a)–(1.3c). Then the stationary point for (1.6) with Lagrange multiplier and the constraint (1.4) satisfies the boundary condition (1.3d) due to Theorem 1, which will be stated in Section 2. Similarly, the energy functional for the interior problem is given by

$$E^i(\omega) = -\frac{1}{2\mu_0}\int_\omega |\nabla u^i|^2 dx + \sigma\int_\Gamma dS \tag{1.7}$$

for a solution u^i to (1.5a)–(1.5c). For the stability and existence of the energy functionals E^o and E^i, we refer the reader to Henrot and Pierre (1990), Dambrine and Pierre (2000), Novruzi (2004) and Barkatou et al. (2006) and references therein. Several numerical methods for the direct problem have been proposed as well, for example, see Shercliff (1981), Pierre and Roche (1991), Coulaud and Henrot (1994) and Novruzi and Roche (1995).

On the other hand, it is a very interesting problem from the practical as well as mathematical points of view to find a configuration of current density j which produces a particular target shape ω. However, only a few results on this inverse problem are known compared to the direct problem. As mentioned earlier, Henrot and Pierre provided the necessary and sufficient conditions for feasible domains in Henrot and Pierre (1989) for a square integrable j. It is, however, a more natural assumption in a laboratory that j is a linear combination of Dirac delta functions. In this case, it is known that there is a domain which can not be shaped although a target shape is smooth enough. Canelas et al. gave numerical solutions to the inverse problems in Canelas et al. (2009b) using the Feasible Arc Interior Point Algorithm. They also used the same method by assuming that the current density is a finite sum of characteristic functions in Canelas et al. (2009a).

In this work, we showed the inverse problem has infinitely many solutions for square integrable j (Proposition 1). The non-uniqueness can be fixed from the assumption that j is a finite sum of Dirac delta functions (Theorems 2 and 3). For the numerical algorithm, we change the equilibrium conditions (1.3d) and (1.5c) to

$$\frac{\partial u}{\partial \nu} = f \quad \text{on } \Gamma$$
$$\frac{\partial u^i}{\partial \nu} = f^i \quad \text{on } \Gamma$$

respectively. Then we can consider our problems as standard inverse source problems of the Poisson equation. Although there are several possible choices to determine the normal data f, f^i from the knowledge of the given domain and the equilibrium conditions (1.3d) and (1.5c), we take f, f^i so that they are smooth and satisfy

$$\int_\Gamma f dS = \int_\Gamma f^i dS = 0$$

assuming Γ has a symmetry. Under these settings, we develop an efficient and fast algorithm to solve the inverse problem based on the idea presented in Kang and Lee (2004). We remark that our algorithm for the inverse problem is non-iterative and direct.

In order to check our numerical solution for the inverse problem, it is necessary to solve the direct problem. Here, we introduce the level set method, which is more accurate than the known solvers. For the general theory of the level set method, we refer the reader to Sethian (1999) and Osher and Fedkiw (2003), see also Allaire et al. (2002) and Allaire et al. (2005) for the level set formulation for the shape optimization. We take the derivative of the energy functional with penalty term as the velocity in the level set equation and this level set equation is able to track the equilibrium domain successfully.

This paper is organized as follows. In Section 2 we describe the basic idea of the level set method to solve the exterior direct problem. The inverse problem is discussed in Section 3. The uniqueness result under certain restrictions as well as a numerical algorithm will be given there. The numerical simulation for the inverse problem is presented in Section 4, based on the algorithm discussed in Section 3. The numerical solutions for the inverse problems are verified by the level set method as well. In Section 5 we adapt the idea for the exterior problem to the interior problem. Some concluding remarks are also drawn in the last section.

2 Level set method

In this section, we solve the exterior direct problem by the level set method. First we define the level set function $\phi(t, x)$ such that

$$\omega(t) = \{x : \phi(t, x) < 0\}$$
$$\Omega(t) = \{x : \phi(t, x) > 0\}$$
$$\Gamma(t) = \{x : \phi(t, x) = 0\}$$

Suppose that the velocity of each point is governed by

$$\frac{dx}{dt} = V(t, x(t)) = v\nu.$$

Since $\nu = \nabla\phi/|\nabla\phi|$, we obtain the standard level set equation,

$$\phi_t + v|\nabla\phi| = 0. \tag{2.1}$$

One of the key issues for the level set method is to determine the velocity vector V or v in the level set equation. To this end, we define an objective functional $E(\omega)$ from the penalty method for (1.6) with constraint $\int_\omega dx = S_0$:

$$\inf_\omega E(\omega)$$
$$E(\omega) = E^o(\omega) + \mu\left(\int_\omega dx - S_0\right)^2, \quad \mu >> 1$$

We consider an equilibrium domain ω, a solution to the direct problem (1.3), as the stationary point of $E(\omega)$. Define

$$\omega_V = \omega + V(\omega)$$

for $V \in W^{1,\infty}(\mathbb{R}^2;\mathbb{R}^2)$. Then we obtain the following Fréchet derivative of $E(\omega)$.

Theorem 1 *Suppose that ω is smooth enough and j is a square integrable function compactly supported in Ω. Then $E(\omega)$ is Fréchet differentiable and*

$$DE(\omega)(V) = \int_\Gamma \left(\frac{1}{2\mu_0}|\nabla u| + \sigma\kappa + 2\mu\left(\int_\omega dx - S_0\right)\right) V\cdot\nu dS \tag{2.2}$$

where u is the unique solution to (1.3a)–(1.3c).

Theorem 1 is a very well-known result. The reader can find the proof from the literature, for instance, see Sokołowski and Zolésio (1992) and Pierre and Roche (1991).

From the gradient method for the optimization of $E(\omega)$, it is natural to define the velocity in the level set equation, (2.1), from $DE(\omega)$:

$$-v = \frac{1}{2\mu_0}|\nabla u| + \sigma\kappa + 2\mu\left(\int_\omega dx - S_0\right) \tag{2.3}$$

and thus the level set equation reads

$$\phi_t - \left[\frac{1}{2\mu_0}|\nabla u|^2 + 2\mu\left(\int_\omega dx - S_0\right)\right]|\nabla\phi| = \sigma\nabla\cdot\left(\frac{\nabla\phi}{|\nabla\phi|}\right)|\nabla\phi| \tag{2.4}$$

since

$$\kappa = \nabla\cdot\frac{\nabla\phi}{|\nabla\phi|}.$$

Then, the updated shape ω_{n+1} is obtained from the level set function ϕ^{n+1}, which may be computed from a simple time stepping algorithm

$$\phi^{n+1} = \phi^n + \Delta t\left[\frac{1}{2\mu_0}|\nabla u_n|^2 + 2\mu\left(\int_{\omega_n} dx - S_0\right)\right]|\nabla\phi^n| + \Delta t\sigma\nabla\cdot\left(\frac{\nabla\phi^n}{|\nabla\phi^n|}\right)|\nabla\phi^n| \tag{2.5}$$

We summarize the algorithm as follows.

Algorithm 1

(1) Extract ω_n from given ϕ^n.
(2) Determine $|\nabla u_n|^2$ from (1.3a)–(1.3c).
(3) Update ϕ^{n+1} from (2.5).
(4) Reinitialize the level set function ϕ^{n+1} to be the signed distance function from

$$\psi_\tau + sign(\phi^{n+1})(|\nabla\psi| - 1) = 0 \tag{2.6a}$$

$$\psi(\tau = 0, x) = \phi^{n+1}(x) \tag{2.6b}$$

All other steps except step (2) can be accomplished from the standard level set technique. Here, we explain how $|\nabla u_n|$ is defined in $\mathbb{R}^2$. Although several methods are known to compute u_n in Ω and to extend to $\mathbb{R}^2$, $|\nabla u_n|$ near the boundary Γ_n is the most critical value for the level set method. Thus we compute $|\nabla u_n|$ at Γ_n only, and then extend it to the value at the closest point of Γ_n. Now, we illustrate the method to compute $|\nabla u_n|$ at Γ_n.

First, we note that

$$|\nabla u_n| = \left|\frac{\partial u_n}{\partial\nu}\right|$$

at the boundary Γ_n since the tangent term vanishes. From the fundamental solution for the Laplacian in $\mathbb{R}^2$, $\Phi(x,y) = -\frac{1}{2\pi}\ln|x-y|$, we define

$$h(x) = -\frac{\mu_0}{2\pi}\int_{\mathbb{R}^2}\ln|x-y|j(y)dy \tag{2.7}$$

Then $h(x)$ solves (1.3a) in Ω_n. Moreover, one can show that $|\partial h/\partial r| = O(1/|x|^2)$ as $|x|\to\infty$ due to the condition (1.2). Thus $\tilde{u} := u_n - h$ solves

$$-\Delta\tilde{u} = 0 \quad \text{in } \Omega_n \tag{2.8a}$$

$$\tilde{u} = -h \quad \text{on } \Gamma_n \tag{2.8b}$$

$$\left|\frac{\partial\tilde{u}}{\partial r}\right| = O\left(\frac{1}{|x|^2}\right) \quad \text{as } |x|\to\infty \tag{2.8c}$$

It follows that

$$\frac{\partial u_n}{\partial\nu} = \frac{\partial\tilde{u}}{\partial\nu} + \frac{\partial h}{\partial\nu}, \quad x\in\Gamma_n \tag{2.9}$$

Since the boundary condition at infinity, (2.8c) implies $\tilde{u} = 0$ as $|x|\to\infty$, there is a unique solution to (2.8). There are several methods to solve the exterior problem (2.8) and the normal derivative $\partial\tilde{u}/\partial\nu =: \tilde{f}$ may be computed from $\tilde{u}$.

Here, we compute $\partial\tilde{u}/\partial\nu$ directly from Calderón's projector (see e.g. Hsiao and Wendland 2008)

$$\tilde{f}(x) + 2\int_{\Gamma_n} \tilde{f}(y)\frac{\partial\Phi(x,y)}{\partial\nu(x)}dS(y) = 2\frac{\partial}{\partial\nu(x)}\int_{\Gamma_n} h(y)\frac{\partial\Phi(x,y)}{\partial\nu(y)}dS(y),\ x\in\Gamma_n \tag{2.10}$$

The existence and uniqueness for these types of integral equations are well known (see e.g. Kress 1999). In general, it has a unique solution if an additional condition

$$\int_{\Gamma_n} \tilde{f}dS = c \tag{2.11}$$

is given. Indeed, for a sufficiently large $B_R := B(0,R)$

$$\int_{B_R\setminus\overline{\omega}_n} \Delta\tilde{u}dx = \int_{\partial B_R}\frac{\partial\tilde{u}}{\partial\nu}dS - \int_{\Gamma_n}\tilde{f}dS.$$

Sending $R\to\infty$ yields that

$$\int_{\Gamma_n}\tilde{f}dS = c = 0$$

from (2.8c). For the numerical implementation, we solve

$$\tilde{f}(x) + 2\int_{\Gamma_n}\tilde{f}(y)\left[\frac{\partial\Phi(x,y)}{\partial\nu(x)}+1\right]dS(y) = 2\frac{\partial}{\partial\nu(x)}\int_{\Gamma_n} h(y)\frac{\partial\Phi(x,y)}{\partial\nu(y)}dS(y),\ x\in\Gamma_n \tag{2.12}$$

since it is equivalent to (2.10) together with (2.11) for $c=0$.

Numerical examples with detailed discretization schemes are provided in Section 4.

3 Inverse shaping problem

In this section we discuss the inverse problem for (1.3) with (1.4). That is, for a given feasible domain ω we seek the current density function j. Unfortunately, infinitely many solutions exist. Indeed, for any smooth function η which is compactly supported in Ω, j and $j-\Delta\eta/\mu_0$ give the same equilibrium domain. We define θ as

$$\theta = -\frac{1}{\mu_0}\Delta\eta. \tag{3.1}$$

Since η has a compact support, it satisfies (1.3c) and

$$\eta = \frac{\partial\eta}{\partial\nu} = 0 \quad \text{on } \Gamma \tag{3.2}$$

It follows that

$$\begin{aligned}
&-\Delta(u+\eta) = \mu_0(j+\theta) \quad \text{in } \Omega\\
&u+\eta = 0 \quad \text{on } \Gamma\\
&\left|\frac{\partial(u+\eta)}{\partial r}\right| = O\left(\frac{1}{|x|^2}\right) \quad \text{as } |x|\to\infty\\
&\frac{1}{2\mu_0}|\nabla(u+\eta)|^2 + \sigma\kappa = P_0 \quad \text{on } \Gamma
\end{aligned}$$

provided u, j, ω and P_0 satisfy (1.3). We summarize as follows.

Proposition 1 *Suppose that for a given target shape ω there exists a function j which solves the inverse problem for (1.3) and (1.4). Then for any θ satisfying (3.1) and (3.2) with a smooth function η which is compactly supported in Ω, $j+\theta$ also solves the inverse problem.*

This non-uniqueness for the inverse problem, however, can be fixed by restricting the class of j. We assume that j is a finite sum of point sources,

$$j = \sum_{p=1}^{m}\beta_p\delta(x-x_p) \tag{3.3}$$

Then the uniqueness up to the sign of the source term is obtained. More precisely, we have the following theorem.

Theorem 2 *Suppose that*

$$j = \sum_{p=1}^{m}\beta_p\delta(x-x_p), \quad m<\infty$$

and

$$j' = \sum_{p=1}^{m'}\beta'_p\delta(x-x'_p), \quad m'<\infty$$

are solutions to the inverse problem (1.3) for given ω and P_0. Then either $j=j'$ or $j=-j'$.

Proof Let u and u' be solutions to (1.3) with the source terms j and j' respectively. Then at the boundary Γ

$$\left|\frac{\partial u}{\partial\nu}\right| = \left|\frac{\partial u'}{\partial\nu}\right| \tag{3.4}$$

We rewrite the boundary condition (3.4) on $\Gamma_1\cup\Gamma_2=\Gamma$ as

$$\begin{aligned}
&\frac{\partial u}{\partial\nu} = \frac{\partial u'}{\partial\nu} \quad \text{on } \Gamma_1\\
&\frac{\partial u}{\partial\nu} = -\frac{\partial u'}{\partial\nu} \quad \text{on } \Gamma_2
\end{aligned}$$

Suppose that $|\Gamma_1| > 0$. Then $w = u - u'$ solves

$$-\Delta w = \mu_0 \sum_{p=1}^{n} \gamma_p \delta(x - y_p) \quad \text{in } \Omega \tag{3.5a}$$

$$w = 0 \quad \text{on } \Gamma \tag{3.5b}$$

$$\left|\frac{\partial w}{\partial r}\right| = O\left(\frac{1}{|x|^2}\right) \quad \text{as } |x| \to \infty \tag{3.5c}$$

$$\frac{\partial w}{\partial \nu} = 0 \quad \text{on } \Gamma_1 \tag{3.5d}$$

where, $j - j' = \sum_{p=1}^{n} \gamma_p \delta(x - y_p)$. We construct a set of harmonic functions in Ω, $\{h_q\}_{q=1}^{n}$ such that

$$h_q(y_p) = \delta_{q,p} \tag{3.6a}$$

$$h_q = 0 \quad \text{on } \Gamma_2 \tag{3.6b}$$

$$\left|\frac{\partial h_q}{\partial r}\right| = O(\frac{1}{|x|^2}) \quad \text{as } |x| \to \infty \tag{3.6c}$$

We apply Green's formula over $G_R := B_R \setminus \overline{\omega}$ for sufficiently large R to obtain

$$\int_{G_R} w\Delta h_q - \Delta w h_q dx = \int_{\partial G_R} w\frac{\partial h_q}{\partial \nu} - \frac{\partial w}{\partial \nu} h_q dS$$

$$\mu_0 \gamma_q = \int_{\partial B_R} w\frac{\partial h_q}{\partial \nu} - \frac{\partial w}{\partial \nu} h_q dS$$

The right hand side converges to 0 as $R \to \infty$ due to the asymptotic behaviors of w, h_q, (3.5d) and (3.6c). Thus, we conclude that $\gamma_q = 0$ for all $q = 1, \cdots, n$ and $j = j'$.

In the case that $|\Gamma_1| = 0$, $w = u + u'$ solves

$$-\Delta w = \mu_0 \sum_{p=1}^{n} \gamma_p \delta(x - y_p) \quad \text{in } \Omega$$

$$w = 0 \quad \text{on } \Gamma$$

$$\left|\frac{\partial w}{\partial r}\right| = O(\frac{1}{|x|^2}) \quad \text{as } |x| \to \infty$$

$$\frac{\partial w}{\partial \nu} = 0 \quad \text{on } \Gamma$$

where $j + j' = \sum_{p=1}^{n} \gamma_p \delta(x - y_p)$. Here we use the same notations for the case of $|\Gamma_1| > 0$ to avoid using too many notations. The idea is very similar to the previous case. From Green's formula with harmonic function h_q satisfying (3.6a) and (3.6c) ((3.6b) is not necessary in this case), it follows that $j + j' = 0$ as desired.

The remaining part of the proof is the existence of harmonic functions $\{h_q\}$ in Ω satisfying (3.6). We assume that $0 \in \omega$ without loss of generality by translation. Then from condition (3.6c) and the Kelvin transform, K, it is enough to find a harmonic function $\tilde{h}_q$ in a bounded domain $\tilde{\Omega}$ such that

$$\tilde{h}_q(\tilde{y}_p) = \delta_{q,p}$$

$$\tilde{h}_q = 0 \quad \text{on } \tilde{\Gamma}_2$$

where $\tilde{y}_p$, $\tilde{\Omega}$, and $\tilde{\Gamma}_2$ are the image of y_p, Ω, and Γ_2 respectively under the Kelvin transform. Define a conformal map F_q such that $\tilde{y}_p$ for $p = 1, \cdots, n$, $p \neq q$ maps to 0 and $\tilde{y}_q$ to a non-zero point, e.g.

$$F_q(z) = \prod_{p \neq q} (z - z_p)$$

where $z = x^{(1)} + ix^{(2)}$, $z_p = \tilde{y}_p^{(1)} + i\tilde{y}_p^{(2)}$. Let g_q be a harmonic function in $F_q(\tilde{\Omega})$ satisfying

$$-\Delta g_q = 0$$

$$g_q = 0 \quad \text{on } F_q(\tilde{\Gamma}_1)$$

$$g_q(0) = 0, \quad g_q(F_q(z_q)) \neq 0$$

One can easily check the existence of such a function g_q from the Riemann mapping theorem and Poisson integral. From the construction,

$$h_q = \frac{g_q \circ F_q \circ K}{(g_q \circ F_q \circ K)(y_q)}$$

is a harmonic function in Ω satisfying (3.6). □

Now we illustrate a numerical algorithm to restore j from the given admissible target shape. In Theorem 2 we assumed that the lagrange multiplier P_0 is given. In the direct problem, we consider P_0 is an unknown variable in general. However, in the inverse problem one may compute P_0 if the given feasible domain is smooth. From the additional boundary condition (1.3d), the normal derivative should be

$$\frac{\partial u}{\partial \nu} = \sqrt{2\mu_0(P_0 - \sigma\kappa)}\, \chi_{\Gamma_+} - \sqrt{2\mu_0(P_0 - \sigma\kappa)}\, \chi_{\Gamma_-}$$

for disjoint sub-boundaries Γ_+ and Γ_- such that $\Gamma = \Gamma_+ \cup \Gamma_-$. Since we assume that the boundary is smooth, so is the

normal derivative at Γ. Assumption (1.2) implies that P_0 is the maximum value of $\sigma\kappa$. Indeed, κ must be attained in an even number of points, which is a necessary condition for the feasible domain as pointed out in Henrot and Pierre (1989). Also the feasible domain has to satisfy

$$\int_{\Gamma_+} \sqrt{2\mu_0(P_0-\sigma\kappa)}dS = \int_{\Gamma_-} \sqrt{2\mu_0(P_0-\sigma\kappa)}dS \quad (3.7)$$

From these conditions, we are able to define a smooth f on Γ by taking $\sqrt{2\mu_0(P_0-\sigma\kappa)}$ with changing its sign at points where $P_0 = \sigma\kappa$. Then the inverse problem for (1.3) would be

$$-\Delta u = \mu_0 j \quad \text{in } \Omega \quad (3.8a)$$

$$u = 0 \quad \text{on } \Gamma \quad (3.8b)$$

$$\left|\frac{\partial u}{\partial r}\right| = O\left(\frac{1}{|x|^2}\right) \quad \text{as } |x| \to \infty \quad (3.8c)$$

$$\frac{\partial u}{\partial \nu} = f \quad \text{on } \Gamma \quad (3.8d)$$

To determine the source term j in the form of (3.3), we apply Green's formula with z^{-n}, $n = 0, 1, 2, \cdots$. Here we can assume that $0 \in \omega$ without loss of generality by translation. Then z^{-n} is a harmonic function in Ω and thus

$$-\int_{G_R} \Delta u z^{-n} dx = -\int_{\partial G_R} \frac{\partial u}{\partial \nu} z^{-n} + u\frac{\partial z^{-n}}{\partial \nu} dS$$

Recall that $G_R := B_R \setminus \overline{\omega}$. From the similar argument as in the proof of Theorem 2, we deduce that

$$\mu_0 \sum_{p=1}^{m} \beta_p (\alpha_p)^{-n} = \int_\Gamma f z^{-n} dS$$

where $\alpha_p = x_p^{(1)} + i x_p^{(2)}$. Now this problem can be understood as the well-known inverse source problem that is seeking

$$\xi(z) = \sum_{p=1}^{m} \frac{\beta_p}{z - 1/\alpha_p}, \quad \alpha_p, \beta_p \in \mathbb{C}, \quad |1/\alpha_p| < R$$

from the measurement of $\xi(z)|_{|z|=R}$. This inverse source problem has been studied in analytically as well as numerically. Here, we apply the numerical method introduced in Kang and Lee (2004). Indeed, α_p, β_p can be recovered in the following manner:

Algorithm 2 (Kang and Lee 2004)

(1) For given m, compute

$$c_n = \int_\Gamma f z^{-n} dS, \quad n = 0, 1, \cdots, 2m-1$$

(2) Solve the system of equations for l_p, $p = 1, \cdots, m$

$$\begin{bmatrix} c_0 & c_1 & \cdots & c_{m-1} \\ c_1 & c_2 & \cdots & c_m \\ \vdots & \vdots & & \vdots \\ c_{m-1} & c_m & \cdots & c_{2m-2} \end{bmatrix} \begin{bmatrix} l_m \\ l_{m-1} \\ \vdots \\ l_1 \end{bmatrix} = \begin{bmatrix} -c_m \\ -c_{m+1} \\ \vdots \\ -c_{2m-1} \end{bmatrix}$$

(3) Find zeros of

$$z^m + l_1 z^{m-1} + \cdots + l_m = 0$$

which are $1/\alpha_1, \cdots, 1/\alpha_m$.

(4) Solve the following equation for $\beta_1, \cdots \beta_m$

$$\begin{bmatrix} 1 & 1 & \cdots & 1 \\ \alpha_1^{-1} & \alpha_2^{-1} & \cdots & \alpha_m^{-1} \\ \vdots & \vdots & & \vdots \\ \alpha_1^{-m+1} & \alpha_2^{-m} & \cdots & \alpha_m^{-2m+2} \end{bmatrix} \begin{bmatrix} \beta_1 \\ \beta_2 \\ \vdots \\ \beta_m \end{bmatrix} = \begin{bmatrix} c_0 \\ c_1 \\ \vdots \\ c_{m-1} \end{bmatrix}$$

4 Numerical examples

Numerical solution procedures for the inverse problem are now presented, based on the methods just discussed. From the given target shape (see Fig. 2), we computed the curvature κ and P_0/σ as the maximum of κ. Then we were able to determine the normal derivative

$$f = \sqrt{2\mu_0\sigma(P_0/\sigma - \kappa)}\chi_{\Gamma_+} - \sqrt{2\mu_0\sigma(P_0/\sigma - \kappa)}\chi_{\Gamma_-} \quad (4.1)$$

by splitting the boundary to $\Gamma_\pm$ at the points where $P_0/\sigma = \kappa$ so that f is smooth and satisfies condition (3.7). Table 1 shows computed α_p, β_p values via Algorithm 2 for various initial guesses of number of point sources. Here α_p and $\mathrm{Re}\,\beta_p$ represent the positions and intensity of point sources and we take $\mu_0 = \sigma = 1$.

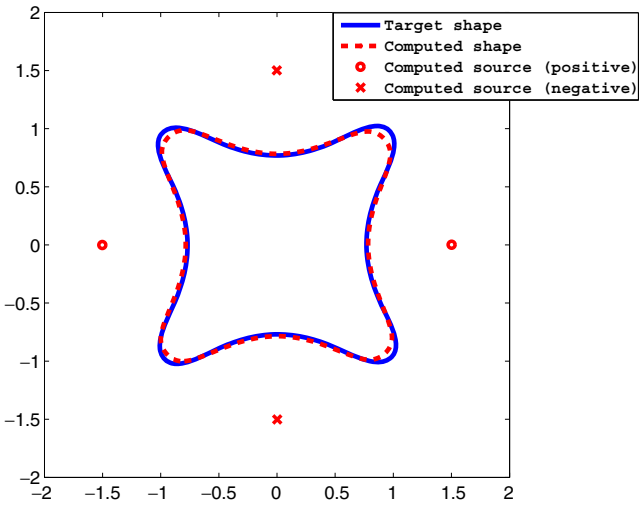

Fig. 2 Example 1: Computed source and shape

The numerical results shown in Table 1 indicate that $m = 4$ is acceptable for the target shape since the intensities are relatively small or the distance of the source from the target is too large to effect a change of shape in the case of $m > 4$. We call these point sources "false sources". If the target shape is a feasible shape from a finite number of sources, the "false source" is originated from approximation error or noise. Thus "false sources" may give a worse image in some cases. For this reason, we call them "false sources". However, if the target shape is not a feasible shape we may improve the computed shape by adding more sources. This result is supported by numerical simulation of the direct problem. Indeed, the target shape can be successively restored from the numerical solution to the inverse problem given in Table 1 as shown in Fig. 2. To solve the direct problem, we used the level set method, Algorithm 1 which was introduced in Section 2. Although it can be improved from various modern level set techniques and high order schemes to discretize the level set equation (2.4) and the integral equation (2.12), we use standard techniques, which are now briefly explained.

(1) **Integral equation:** To solve the integral equation (2.12) numerically, we apply the idea described in Kress (1998, 1999). We assume that the boundary Γ_n possesses a 2π-periodic parametric representation of the form

$$x(t) = (x^{(1)}(t), x^{(2)}(t)), \ 0 \le t \le 2\pi$$

in a counterclockwise orientation satisfying $|dx/dt| > 0$ for all t. Then the integral equation (2.12) can be rewritten as

$$w(t) + \int_0^{2\pi} w(\tau) K(t,\tau) d\tau = -H(t) \tag{4.2}$$

Here $w(t) = \tilde{f}(x^{(1)}(t), x^{(2)}(t))$, the kernel $K = K_1 + K_2$ is defined as

$$K_1(t,\tau) = \begin{cases} \dfrac{1}{\pi} \dfrac{dx}{dt} \dfrac{x(t) - y(\tau)}{|x(t) - y(\tau)|^2} \left| \dfrac{dy/d\tau}{dx/dt} \right| & t \neq \tau \\ \dfrac{1}{2\pi} \dfrac{dx^2}{d^2t} \dfrac{dx/dt}{|dx/dt|^2} & t = \tau \end{cases}$$

$$K_2(\tau) = 2|dy/d\tau|$$

Table 1 Example 1: Computed positions and intensities of point sources

m	α	β	m	α	β
4	$\mathbf{-1.5015 - 0.0021i}$	$12.9195 + 0.0564i$	**5**	$\mathbf{-1.5015 - 0.0021i}$	$12.9195 + 0.0564i$
	$\mathbf{0.0021 - 1.5015i}$	$-12.9195 - 0.0564i$		$\mathbf{0.0021 - 1.5015i}$	$-12.9195 - 0.05641i$
	$\mathbf{1.5015 + 0.0021i}$	$12.9195 + 0.0564i$		$\mathbf{1.5015 + 0.0021i}$	$12.9194 + 0.05623i$
	$\mathbf{-0.0021 + 1.5015i}$	$-12.9195 - 0.0565i$		$\mathbf{-0.0021 + 1.5015i}$	$-12.9195 - 0.0564i$
				$1.4720 + 0.4066i$	$0.0001 + 0.0002i$
8	$\mathbf{-1.5124 + 0.0031i}$	$13.2707 - 0.0562i$	**11**	$\mathbf{-1.4925 + 0.0306i}$	$12.6175 - 2.3263i$
	$\mathbf{-0.0031 - 1.5124i}$	$-13.2707 + 0.0562i$		$\mathbf{-0.0306 - 1.4925i}$	$-12.6174 + 2.3261i$
	$\mathbf{1.5124 - 0.0031i}$	$13.2707 - 0.0562i$		$\mathbf{1.4925 - 0.0306i}$	$12.6177 - 2.3250i$
	$\mathbf{0.0031 + 1.5124i}$	$-13.2707 + 0.0562i$		$\mathbf{0.0306 + 1.4925i}$	$-12.6176 + 2.3266i$
	$-1.0527 + 0.8231i$	$-0.0134 + 0.1284i$		$1.2607 - 0.3059i$	$0.2822 + 0.1856i$
	$-0.8231 - 1.0527i$	$0.0134 - 0.1284i$		$-0.3059 - 1.2607i$	$-0.2825 - 0.1858i$
	$0.8231 + 1.0527i$	$0.0134 - 0.1284i$		$0.3059 + 1.2608i$	$-0.2826 - 0.1859i$
	$1.0527 - 0.8231i$	$-0.0134 + 0.1284i$		$-1.2607 + 0.3059i$	$0.2825 + 0.1858i$
				$18.3741 + 26.7455i$	$-825.0073 - 410.5541i$
				$13.3303 - 29.9291i$	$761.6582 - 533.7619i$
				$-33.2026 + 2.7973i$	$63.3493 + 944.3148i$

and the inhomogeneous term $H(t)$ is given by

$$\frac{1}{2\pi|dx/dt|}\int_0^{2\pi}\frac{dh(y(\tau))}{d\tau}\left[2\frac{dx}{dt}\frac{x(t)-y(\tau)}{|x(t)-y(\tau)|^2}\right]d\tau. \tag{4.3}$$

We use the collocation method to approximate (4.2). Indeed, for the Lagrange basis

$$L_i(t)=\frac{1}{2n}(1+2\sum_{k=1}^{n-1}\cos k(t-t_i)+\cos n(t-t_i)),$$

we obtain

$$r_{i+1}+\sum_{j,k}K(t_{i+1},t_j)\left(\int_0^{2\pi}L_j(\tau)L_k(\tau)d\tau\right)r_k = -H(t_{j+1})$$

where

$$w(t)\approx\sum_{i=0}^{2n-1}r_iL_i(t).$$

Note that we split $2dx/dt\cdot(x(t)-y(\tau))/|x(t)-y(\tau)|^2$ in (4.3) as

$$\left[2\frac{dx}{dt}\frac{x(t)-y(\tau)}{|x(t)-y(\tau)|^2}+\cot\frac{\tau-t}{2}\right]-\left[\cot\frac{\tau-t}{2}\right]$$

in order to evaluate $H(t_{j+1})$.

(2) **Level set equation:** First order backward Euler time stepping applied to (2.4) gives (2.5). For the spatial discretization, Godunov's method and second order finite difference formula were used. In one space dimension, these schemes yield

$$\phi_i^{n+1}=\phi_i^n-\Delta t\left[\max(a_i^n,0)G_i^{n,+}+\min(a_i^n,0)G_i^{n,-}-\frac{\phi_{i+1}^n-2\phi_i^n+\phi_{i-1}^n}{(\Delta x)^2}\right]$$

where

$$G_i^{n,+}=\sqrt{\max(\max(D_x^-\phi_i^n,0)^2,\min(D_x^+\phi_i^n,0)^2)}$$
$$G_i^{n,-}=\sqrt{\max(\min(D_x^-\phi_i^n,0)^2,\max(D_x^+\phi_i^n,0)^2)}$$

with

$$D_x^+\phi_i^n=\frac{\phi_{i+1}^n-\phi_i^n}{\Delta x},\quad D_x^-\phi_i^n=\frac{\phi_i^n-\phi_{i-1}^n}{\Delta x}.$$

(3) **Reinitialization equation:** Several numerical methods for the reinitialization step, (2.6), are known. Here, we use Godunov's method after numerical approximation of the sign function to

$$sign(\phi^{n+1})\approx\frac{\phi^{n+1}}{\sqrt{(\phi^{n+1})^2+(\Delta x)^2}}$$

Then, the discretization of reinitialization equation can be written as

$$\psi_i^{n+1}=\psi_i^n-\Delta t\left[\max(S_i,0)F_i^{n,+}+\min(S_i,0)F_i^{n,-}-S_i\right]$$

where $S_i=\phi_i^{n+1}/\sqrt{(\phi_i^{n+1})^2+(\Delta x)^2}$ and similar to $G_i^{n,\pm}$, $F_i^{n,\pm}$ are defined as

$$F_i^{n,+}=\sqrt{\max(\max(D_x^-\psi_i^n,0)^2,\min(D_x^+\psi_i^n,0)^2)}$$
$$F_i^{n,-}=\sqrt{\max(\min(D_x^-\psi_i^n,0)^2,\max(D_x^+\psi_i^n,0)^2)}$$

At each time step, we capture the zero level set curve using a MATLAB function and reparameterize the curve uniformly by a cubic spline.

In Example 1 (Fig. 2), the computed shape is obtained after 300 iteration steps with $\Delta x^{(1)}=\Delta x^{(2)}=0.0234$, $\Delta t=\Delta x^2/4$, and the unit circle as the initial guess. In the level set method, an ideal stopping criterion would be to check the convergence of zero level set curve, but it is difficult to implement. As a consequence, one may try to identify the desired feature of the underlying problem and explore some reasonable stopping criterion. Here we are tracking the length of the zero level set curve to check the convergence. See Fig. 3 for an evolution of shapes and Fig. 4 for the residuals of the arc length. Also we remark that the initial shape may not be a critical point in our approach at least it is smooth and convex with a reasonable size, although the initial guess may make some difference in practice. Figure 5 shows an evaluation of shapes with a different initial shape for Example 1. Another issue in numerical implementation is the choice of the penalty term μ. It is related to the intensities and distances of the sources. If the total power acting on the molten material is increasing then a higher μ needs to be taken. In this example, we take $\mu=700$.

Table 2 shows computed positions and intensities of point sources for a more complicated target shape (see Fig. 6) assuming $m=20$. Due to the weak intensity, only 8 points may be considered as the source. Indeed, Fig. 6, which shows reconstructed shapes from 8 and 20 source points via the level set method, indicates that the other 12 points

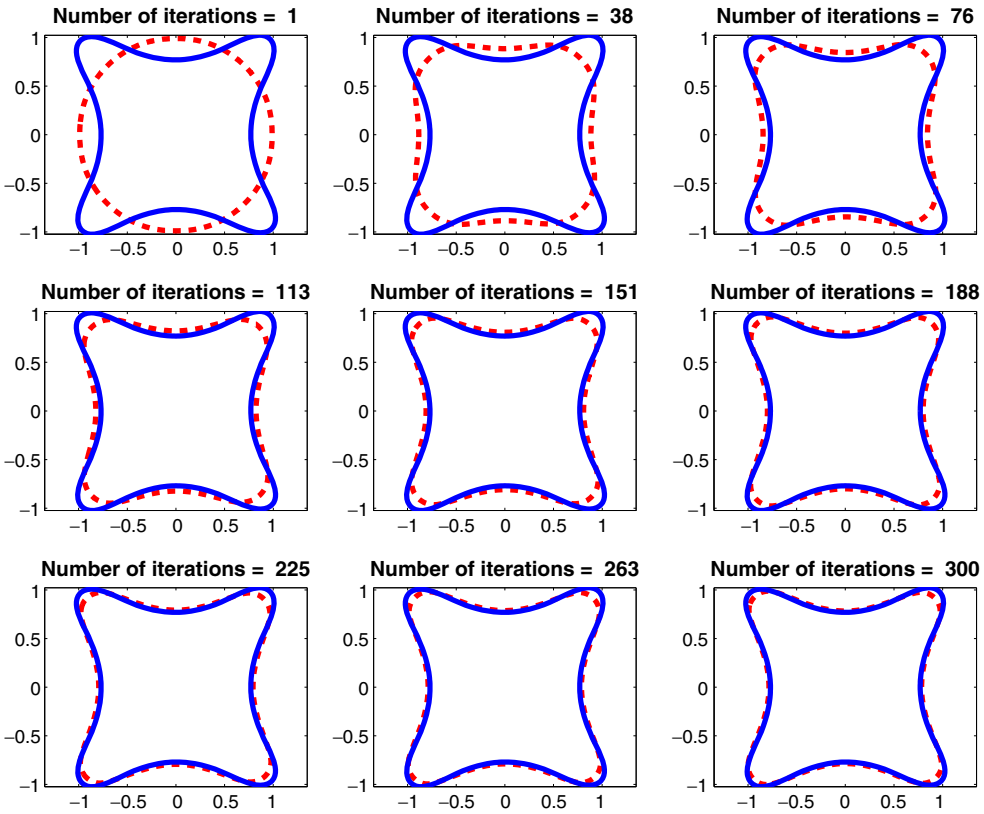

Fig. 3 Example 1: Evolution of shapes

are "false sources". We provide the evolution of shapes and residuals of arc length in Figs. 7 and 8, respectively in the case of 8 points. Here we use $\Delta x^{(1)} = \Delta x^{(2)} = 0.0313$, $\Delta t = \Delta x^2/4$, and $\mu = 100$.

5 Interior shaping problem

In this section, we briefly discuss the interior problem governed by (1.5). A simple modification of the proof for Theorem 2 gives the uniqueness for the interior inverse problem.

Theorem 3 *Suppose that*

$$j = \sum_{p=1}^{m} \beta_p \delta(x - x_p), \quad m < \infty$$

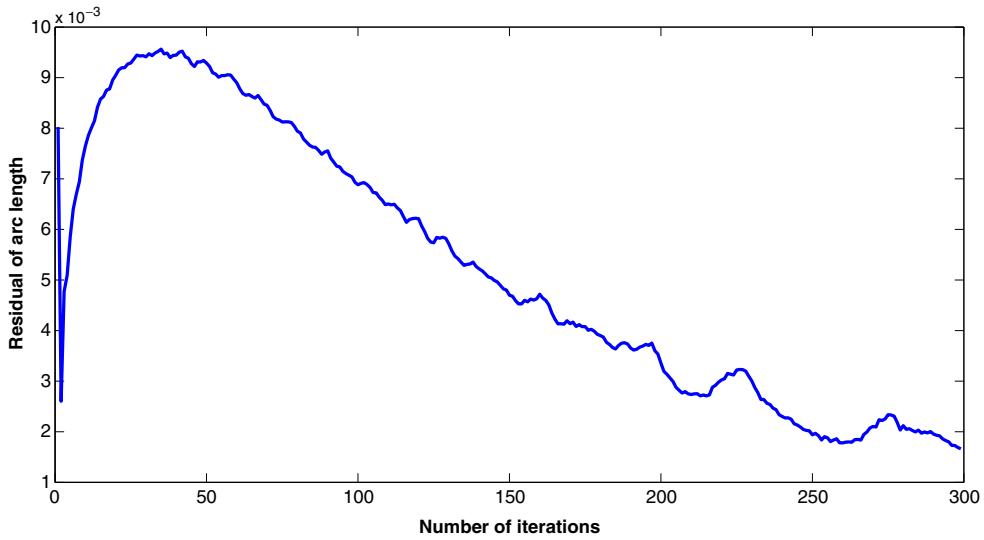

Fig. 4 Example 1: Residuals of arc length

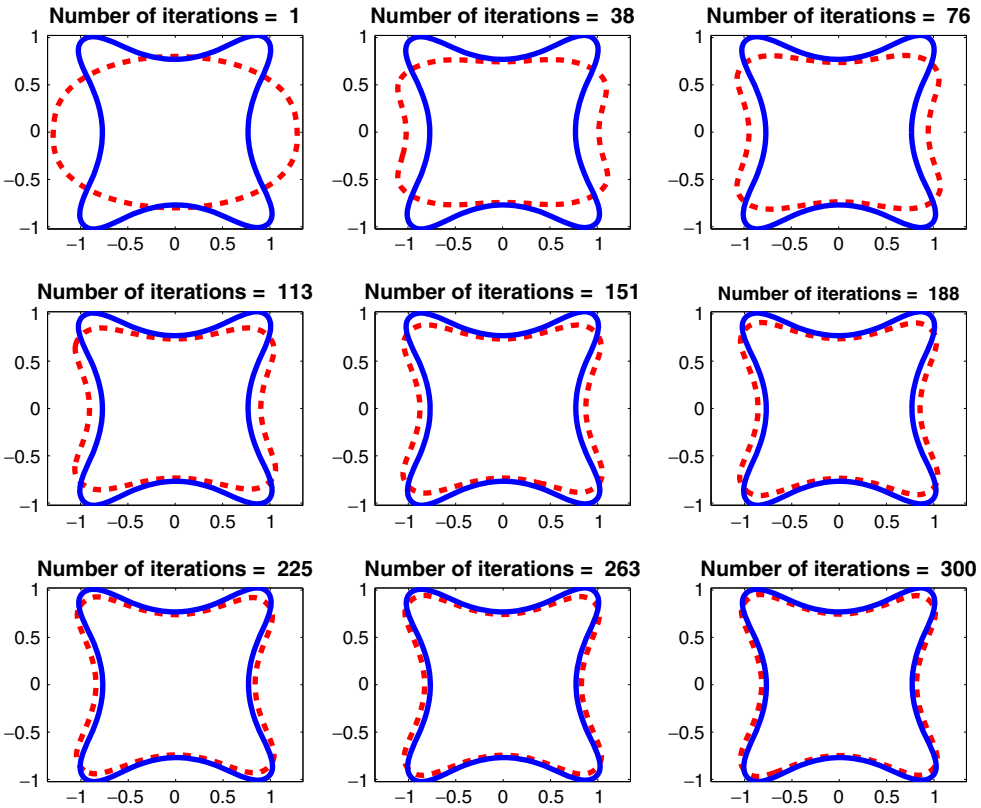

Fig. 5 Example 1: Evolution of shapes with a different initial shape

and

$$j' = \sum_{p=1}^{m'} \beta'_p \delta(x - x'_p), \quad m' < \infty$$

are solutions to the inverse problem (1.5) *for given* ω *and* P_0. *Then either* $j = j'$ *or* $j = -j'$.

We are also able to recover the source term j from the similar algorithm described in the previous section. The only difference is that

$$c_n = \int_\Gamma f^i z^n dS$$

in the first step of Algorithm 2, and thus we can recover (α_p, β_p) instead of $(1/\alpha_p, \beta_p)$ from Algorithm 2.

Table 3 shows the computed intensities and positions of acceptable 24 sources out of 60 for the target shape, known as Kite shape (see Fig. 9). Similar to (4.1) we define

$$f^i = \sqrt{2\mu_0\sigma(P_0/\sigma + \kappa)}\chi_{\Gamma_+} - \sqrt{2\mu_0\sigma(P_0/\sigma + \kappa)}\chi_{\Gamma_-} \tag{5.1}$$

and take P_0 as the minimum of κ with $\mu_0 = \sigma = 1$. This result is verified by numerical simulation. In Fig. 9, we compare the actual shape and recovered shape from

Table 2 Example 2: Computed positions and intensities of point sources

α	β	α	β
$-0.4947 - 0.3433i$	$-0.0000 - 0.0000i$	$-0.6386 - 0.1123i$	$0.0000 + 0.0000i$
$0.6205 + 0.1446i$	$0.0000 - 0.0000i$	$0.5435 + 0.3594i$	$0.0000 + 0.0000i$
$-0.9870 - 0.0221i$	$-0.0000 - 0.0001i$	$-1.1681 + 0.3220i$	$-0.0007 - 0.0149i$
$\mathbf{-1.5014 - 0.0008i}$	$-7.8130 + 0.0155i$	$-1.2193 - 0.8635i$	$0.0187 + 0.0375i$
$\mathbf{-0.9806 - 1.4899i}$	$-2.4207 - 0.1477i$	$\mathbf{0.0044 - 1.5003i}$	$-2.6296 - 0.1121i$
$0.4433 - 1.2023i$	$-0.0009 - 0.0009i$	$1.0531 + 0.0174i$	$0.0003 + 0.0004i$
$1.1625 - 0.3327i$	$0.0026 + 0.0128i$	$\mathbf{0.9966 - 1.5404i}$	$-2.8948 + 0.1672i$
$\mathbf{1.5016 + 0.0017i}$	$7.8132 + 0.0056i$	$-0.4140 + 1.1930i$	$0.0009 + 0.0003i$
$\mathbf{-0.9969 + 1.5385i}$	$2.8785 - 0.1578i$	$\mathbf{-0.0042 + 1.5002i}$	$2.6269 + 0.1072i$
$1.1686 + 0.8772i$	$-0.0039 - 0.0303i$	$\mathbf{0.9821 + 1.4874i}$	$2.4223 + 0.1173i$

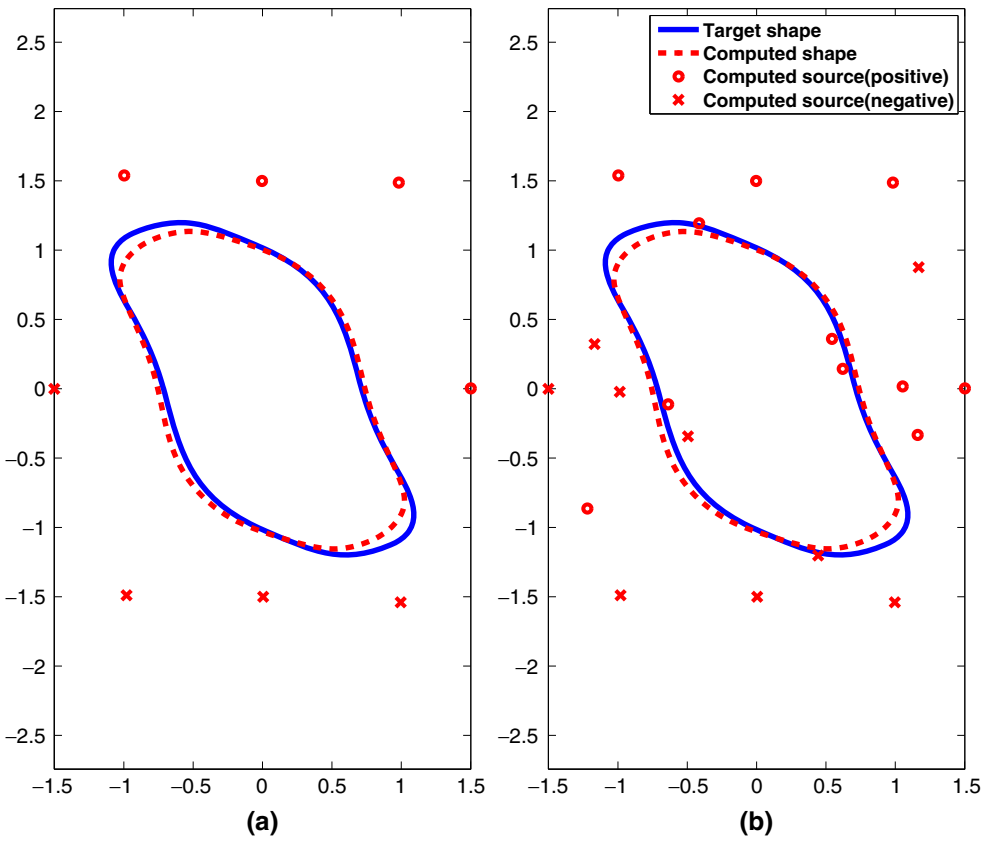

Fig. 6 Example 2: Computed sources and shapes with **a** 8 source points, **b** 20 sources points

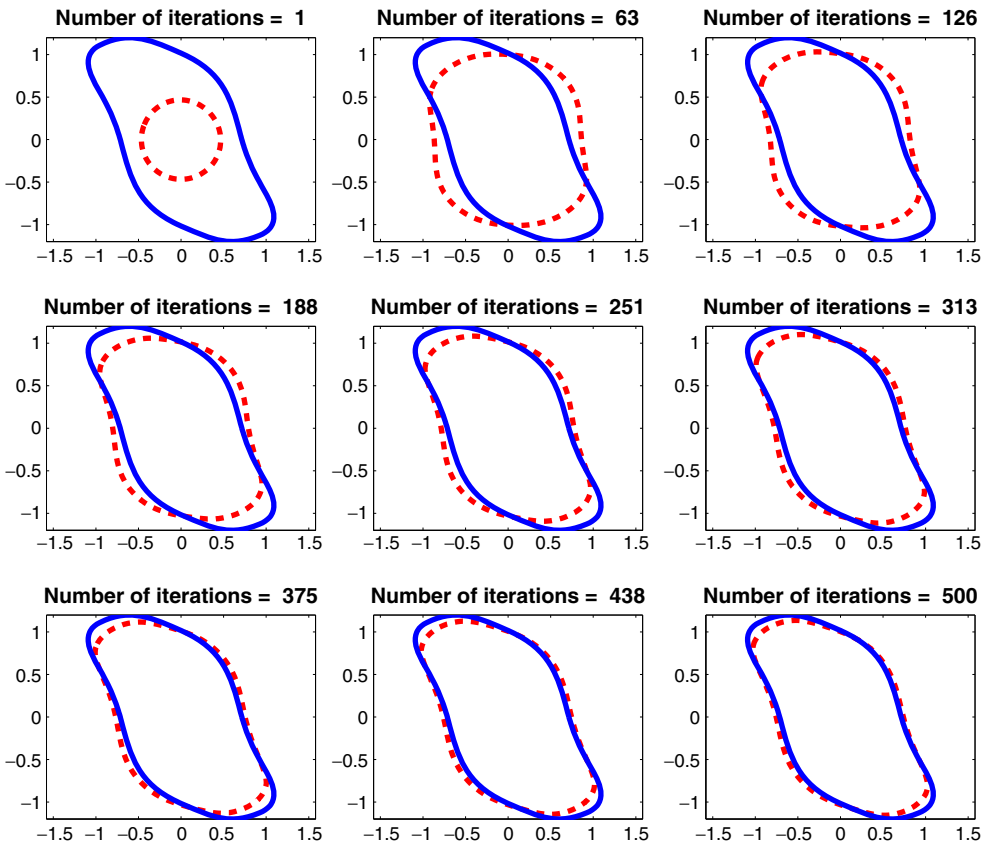

Fig. 7 Example 2: Evolution of shapes for the case of 8 points

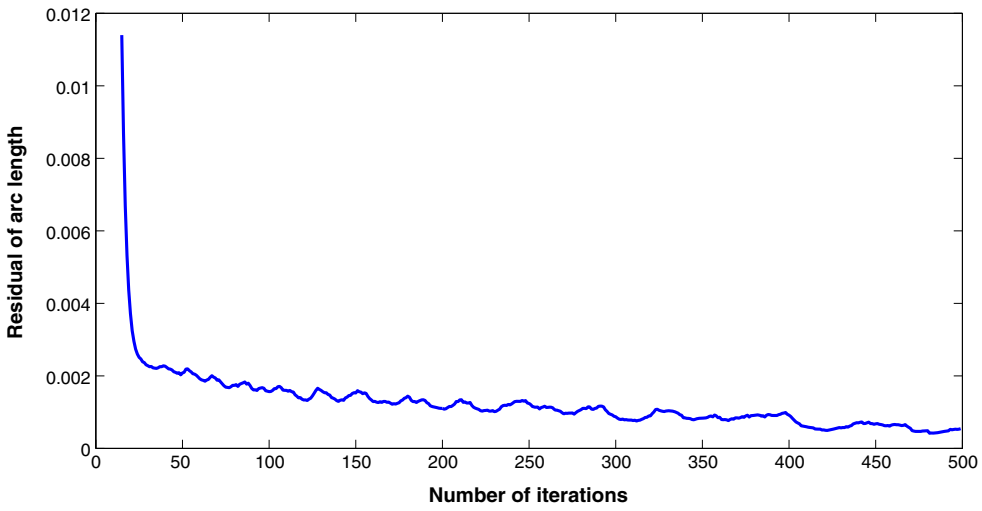

Fig. 8 Example 2: Residuals of arc length for the case of 8 points

Table 3 Example 3: Computed positions and intensities of point sources

α	β	α	β
$-0.7169 - 0.5407i$	$-0.2852 - 0.0265i$	$-0.7127 - 0.5366i$	$-0.2051 - 0.0206i$
$-0.7039 - 0.5282i$	$-0.1807 - 0.0216i$	$-0.6903 - 0.5151i$	$-0.1701 - 0.0261i$
$-0.6718 - 0.4972i$	$-0.1686 - 0.0331i$	$-0.6481 - 0.4739i$	$-0.1741 - 0.0422i$
$-0.6190 - 0.4447i$	$-0.1851 - 0.0535i$	$-0.5840 - 0.4081i$	$-0.2006 - 0.0687i$
$-0.5425 - 0.3624i$	$-0.2203 - 0.0908i$	$-0.4940 - 0.3044i$	$-0.2445 - 0.1260i$
$-0.7169 + 0.5406i$	$0.2967 - 0.0283i$	$-0.7122 + 0.5361i$	$0.2137 - 0.0222i$
$-0.7024 + 0.5266i$	$0.1890 - 0.0237i$	$-0.6873 + 0.5118i$	$0.1795 - 0.0292i$
$-0.6664 + 0.4915i$	$0.1800 - 0.0376i$	$-0.6397 + 0.4649i$	$0.1883 - 0.0485i$
$-0.6066 + 0.4311i$	$0.2019 - 0.0631i$	$-0.5672 + 0.3883i$	$0.2192 - 0.0846i$
$-0.5217 + 0.3335i$	$0.2373 - 0.1199i$	$-0.4373 - 0.2283i$	$-0.2762 - 0.1898i$
$-0.4725 + 0.2613i$	$0.2434 - 0.1837i$	$-0.3711 - 0.1182i$	$-0.3249 - 0.3557i$
$-0.4336 + 0.1692i$	$0.1688 - 0.2269i$	$-0.3840 + 0.0813i$	$0.3228 - 0.2662i$

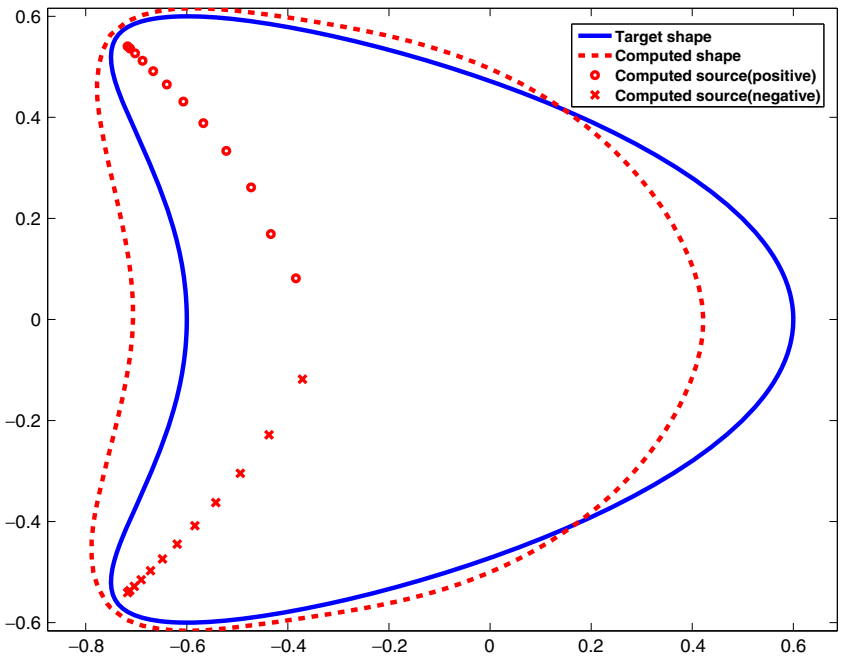

Fig. 9 Example 3: Computed source and shape

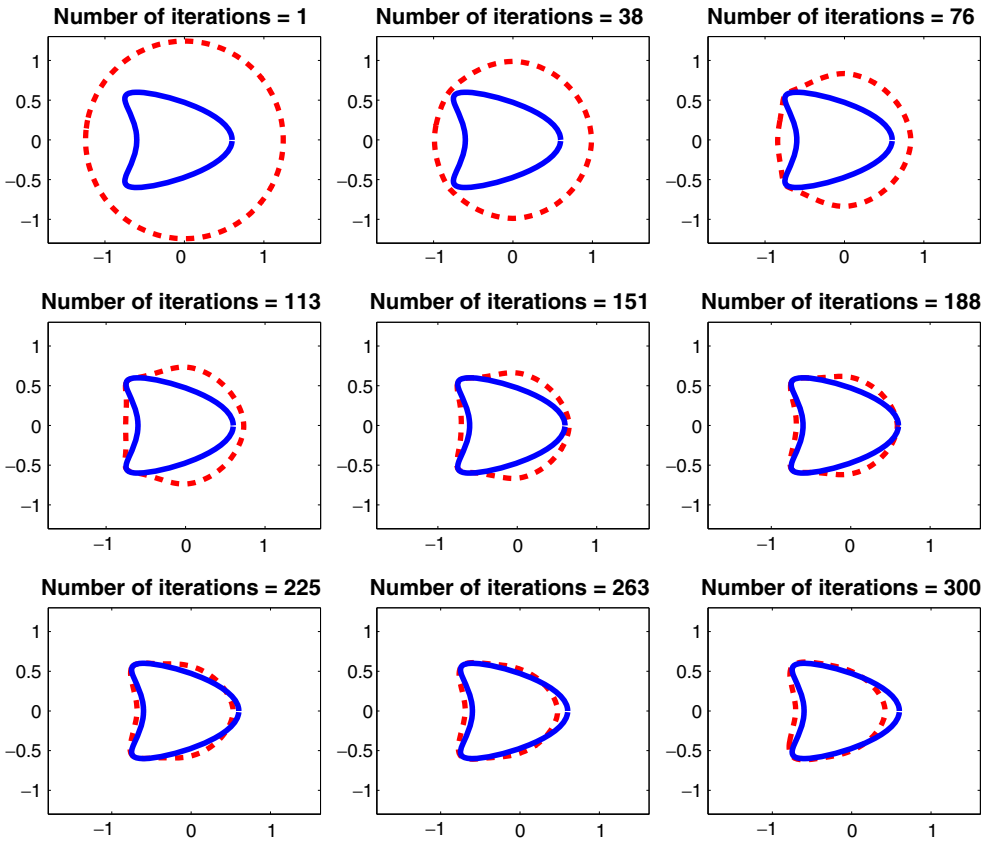

Fig. 10 Example 3: Evolution of shapes

the numerical solution to the inverse problem. We modify the level set method for the exterior problem to solve the direct interior problem. Indeed, the velocity in the level set equation for the interior problem is given by

$$-v^i = -\frac{1}{2\mu_0}|\nabla u^i| + \sigma\kappa + 2\mu\left(\int_\omega dx - S_0\right)$$

and the integral equation (2.12) is also changed to

$$\tilde{f}^i(x) - 2\int_{\Gamma_n} \tilde{f}^i(y)\frac{\partial\Phi(x,y)}{\partial\nu(x)}dS(y) = -2\frac{\partial}{\partial\nu(x)}\int_{\Gamma_n} h(y)\frac{\partial\Phi(x,y)}{\partial\nu(y)}dS(y),\ x\in\Gamma_n$$

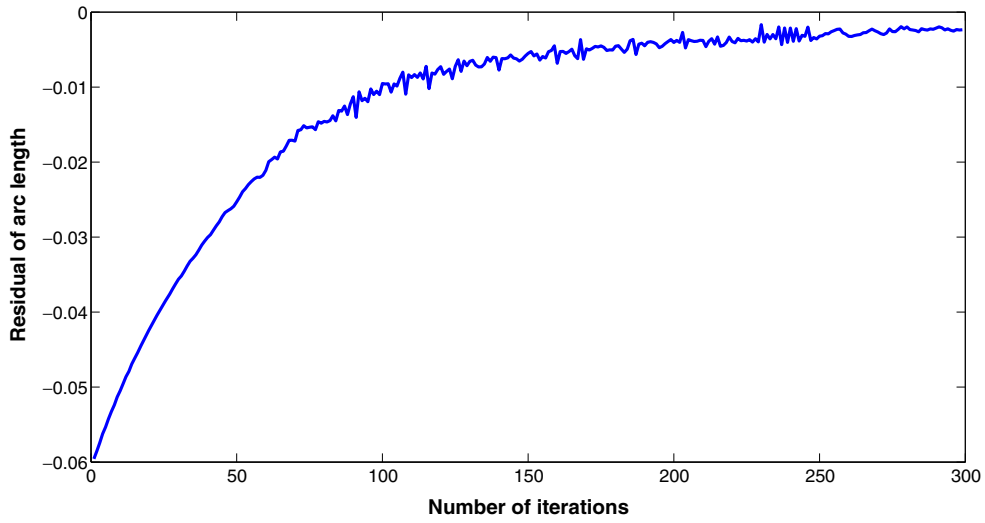

Fig. 11 Example 3: Residuals of arc length

Table 4 Example 4: Computed positions and intensities of point sources

m	α	β	m	α	β
2	$\mathbf{0.2808 + 0.0011i}$	$-14.7283 + 0.1120i$	**3**	$\mathbf{0.2808 + 0.0011i}$	$-14.7283 + 0.1120i$
	$\mathbf{-0.2808 - 0.0011i}$	$14.7283 - 0.1120i$		$\mathbf{-0.2808 - 0.0011i}$	$14.7283 - 0.1120i$
				$(11.1708 + 7.1949i)10^{13}$	$0.0000 + 0.0000i$
6	$\mathbf{0.2958 + 0.0000i}$	$-13.0906 + 0.0007i$	**8**	$\mathbf{0.2959 + 0.0000i}$	$-13.0862 + 0.0001i$
	$\mathbf{-0.2958 - 0.0000i}$	$13.0906 - 0.0007i$		$\mathbf{-0.2959 - 0.0000i}$	$13.0862 - 0.0001i$
	$-0.0066 - 0.2719i$	$-0.0134 - 0.4400i$		$0.0066 + 0.2826i$	$0.0091 + 0.2567i$
	$-0.0041 - 0.1686i$	$-0.0303 - 0.8515i$		$0.0059 + 0.2199i$	$0.0070 + 0.5787i$
	$0.0066 + 0.2719i$	$0.0134 + 0.4400i$		$0.0048 + 0.1187i$	$0.0291 + 0.5440i$
	$0.0041 + 0.1686i$	$0.0303 + 0.8515i$		$-0.0066 - 0.2826i$	$-0.0091 - 0.2567i$
				$-0.0059 - 0.2199i$	$-0.0070 - 0.5787i$
				$-0.0048 - 0.1187i$	$-0.0291 - 0.5440i$

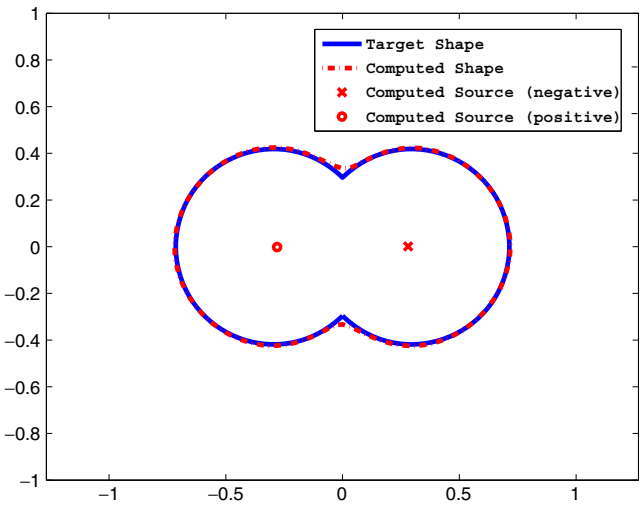

Fig. 12 Example 4: Computed source and shape

which leads to

$$w^i(t) + \int_0^{2\pi} w^i(\tau) K_1(t,\tau) d\tau = H(t)$$

The recovered shape in Fig. 9 is obtained after 300 iteration steps. See also Figs. 10 and 11 for the convergence history. Here we use $\Delta x^{(1)} = \Delta x^{(2)} = 0.0313$, $\Delta t = \Delta x^2/4$, and $\mu = 5$.

Next, we consider an example which has singularities. Table 4 shows the solution to the inverse problem for the target shape, which is a union of two circles centered at $(\pm 1/\sqrt{3\pi + 2}, 0)$ with radius $\sqrt{2/(3\pi + 2)}$ as shown in Fig. 12. We let $\Gamma_\pm$ denote the boundaries of the domain in the right and left half plains. We define the normal derivative as

$$f^i = \sqrt{2\mu_0\sigma(P_0/\sigma + \kappa)}\chi_{\Gamma_+} - \sqrt{2\mu_0\sigma(P_0/\sigma + \kappa)}\chi_{\Gamma_-} \tag{5.2}$$

Table 5 Example 5: Computed positions and intensities of point sources

m	α	β	m	α	β
2	$-0.3531 - 0.0000i$	$-9.8143 + 0.0000i$	**8**	$-0.2959 + 0.0000i$	$-13.0852 - 0.0000i$
	$0.3531 - 0.0000i$	$-9.8143 - 0.0000i$		$0.2959 + 0.0000i$	$-13.0852 + 0.0000i$
4	$-0.2981 - 0.0000i$	$-12.6512 + 0.0000i$		$-0.0000 + 0.2787i$	$0.3346 - 0.0000i$
	$0.2981 - 0.0000i$	$-12.6512 - 0.0000i$		$-0.0000 + 0.2039i$	$0.9850 - 0.0000i$
	$0.0000 - 0.1870i$	$2.8369 - 0.0000i$		$-0.0000 - 0.2787i$	$0.3346 + 0.0000i$
	$-0.0000 + 0.1870i$	$2.8369 + 0.0000i$		$-0.0000 - 0.2039i$	$0.9850 + 0.0000i$
				$-0.0000 + 0.0761i$	$1.9513 - 0.0000i$
				$-0.0000 - 0.0761i$	$1.9513 + 0.0000i$

with $\kappa = \sqrt{(3\pi + 2)/2}$ and $\mu_0 = \sigma = 1$, although Γ has singularities at the intersections of the two circles where κ does not exist. Note that in this example, we cannot determine P_0 since the curvature is not smooth. Indeed, one may compute the inductors for any $P_0 > 0$, which gives the same target shape from a simple change of variables. However, for less P_0 values, the rate of convergence for the direct problem would be slow. Here we take $P_0 = 10$. Similar to other examples, there are false sources for $m > 2$ as indicated in Table 4. The numerical result for $m = 2$ is verified by the solution to the direct problem as shown in Fig. 12.

We remark that condition (1.2) is not required in the interior problem. Indeed, (1.2) is essential for the uniqueness for the exterior boundary value problems. However, in the case of the interior problem, this condition can be removed. As a consequence, $\int_\Gamma f^i dS$ needs not vanish and this is convenient for defining the normal derivative f^i. For example, for the target shape given above we can specify the normal derivative as a constant,

$$f^i = \sqrt{2\mu_0\sigma(P_0/\sigma + \kappa)}$$

Table 5 shows that computed α_p, β_p with this f^i. In this case, there are no false sources and a large number of source points may be needed to restore the target shape as shown in Fig. 13. Indeed, the uniqueness result, Theorem 3, implies that infinitely many sources are required in this approach if the target is a feasible shape by a finite number of source points.

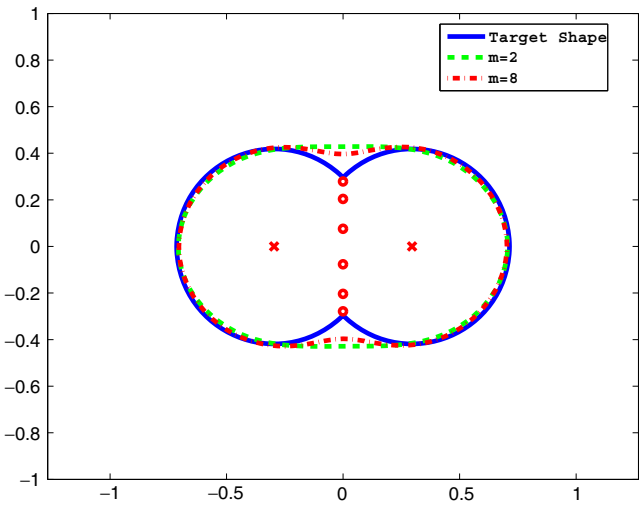

Fig. 13 Example 5: Computed source and shape. The indicated source points are for the case $m = 8$

6 Conclusion

In this paper we discussed the exterior and interior inverse problems arising from magnetic shape forming in 2-dimensional space. We showed for a given target shape there are at most two density functions, j and $-j$, generating the given shape if the density function is known a priori by a finite sum of point sources and the total density is 0. Under these assumptions we proposed a numerical algorithm based on the idea in Kang and Lee (2004), through which we were able to recover the density functions for admissible target shapes. We remark that our algorithm for the inverse problem is a non-iterative and direct method. Our numerical results have been verified by comparing the given target shapes and the numerical solutions to the direct problem from computed source terms. As for the direct problem solver, we introduced the level set method. The level set approach for the direct problem is more applicable and of interest itself mathematically.

It is an interesting and challenging problem as well as an important problem from a practical point of view to solve the inverse problem for arbitrary domains or non-admissible domains. In this case, we have to carefully define the normal derivative $\partial u/\partial \nu$ and then apply our algorithm to restore the current density function in some optimal sense, which is our ongoing work.

References

Allaire G, Jouve F, Toader A-M (2002) A level-set method for shape optimization. C R Math Acad Sci Paris 334(12):1125–1130

Allaire G, de Gournay F, Jouve F, Toader A-M (2005) Structural optimization using topological and shape sensitivity via a level set method. Control Cybern 34(1):59–80

Barkatou M, Seck D, Ly I (2006) An existence result for an interior electromagnetic casting problem. Cent Eur J Math 4(4):573–584 (electronic)

Canelas A, Roche JR, Herskovits J (2009a) Inductor shape optimization for electromagnetic casting. Struct Multidisc Optim 39(6):589–606

Canelas A, Roche JR, Herskovits J (2009b) The inverse electromagnetic shaping problem. Struct Multidisc Optim 38(4):389–403

Coulaud O, Henrot A (1994) Numerical approximation of a free boundary problem arising in electromagnetic shaping. SIAM J Numer Anal 31(4):1109–1127

Crouzeix M (1991) Variational approach of a magnetic shaping problem. Eur J Mech B Fluids 10(5):527–536

Dambrine M, Pierre M (2000) About stability of equilibrium shapes. M2AN Math Model Numer Anal 34(4):811–834

Henrot A, Pierre M (1989) Un problème inverse en formage des métaux liquides. RAIRO Modél Math Anal Numér 23(1): 155–177

Henrot A, Pierre M (1990) About critical points of the energy in an electromagnetic shaping problem. In: Boundary control and boundary variation (Sophia-Antipolis, 1990), Lecture notes in control and inform. sci., vol 178. Springer, Berlin, pp 238–252

Hsiao GC, Wendland WL (2008) Boundary integral equations. In: Applied mathematical sciences, vol 164. Springer, Berlin

Kang H, Lee H (2004) Identification of simple poles via boundary measurements and an application of EIT. Inverse Probl 20(6):1853–1863

Kress R (1998) Numerical analysis. In: Graduate texts in mathematics, vol 181. Springer, New York

Kress R (1999) Linear integral equations. In: Applied mathematical sciences, vol 82, 2nd edn. Springer, New York

Novruzi A (2004) $C^{2,\alpha}$ existence result for a class of shape optimization problems. SIAM J Control Optim 43(1):174–193 (electronic)

Novruzi A, Roche JR (1995) Second order derivatives, Newton method, application to shape optimization. Research Report RR-2555, INRIA

Osher S, Fedkiw R (2003) Level set methods and dynamic implicit surfaces. In: Applied mathematical sciences, vol 153. Springer, New York

Pierre M, Roche J-R (1991) Computation of free surfaces in the electromagnetic shaping of liquid metals by optimization algorithms. Eur J Mech B Fluids 10(5):489–500

Pierre M, Roche J-R (1993) Numerical simulation of tridimensional electromagnetic shaping of liquid metals. Numer Math 65(2):203–217

Pierre M, Rouy E (1996) A tridimensional inverse shaping problem. Commun Partial Differ Equ 21(7–8):1279–1305

Sethian JA (1999) Level set methods and fast marching methods. In: Cambridge monographs on applied and computational mathematics, vol 3, 2nd edn. Cambridge University Press, Cambridge. Evolving interfaces in computational geometry, fluid mechanics, computer vision, and materials science

Shercliff JA (1981) Magnetic shaping of molten metal columns. Proc R Soc Lond, A 375:455–473

Sokołowski J, Zolésio J-P (1992) Introduction to shape optimization. In: Springer series in computational mathematics, vol 16. Springer, Berlin. Shape sensitivity analysis